Numerical Study of Sandbar Migration under Wave-Undertow Interaction

Jinhai Zheng[1]; Chi Zhang[2]; Zeki Demirbilek, F.ASCE[3]; and Lihwa Lin, M.ASCE[4]

Abstract: Reliable simulation of onshore-offshore sandbar migration under various wave and current conditions has remained a challenging task over the last three decades because wave-undertow interaction in the surf zone has been neglected in the existing numerical models. This paper presents the development of an improved sandbar migration model using a phase- and depth-resolving modeling approach. This new model includes interactions between waves and undertow and an empirical time-dependent turbulent eddy viscosity formulation that accounts for the phase dependency of turbulence on flow velocity and acceleration. The authors demonstrate through extensive model-data comparisons that these enhancements resulted in significant improvements in the predictive capability of the cross-shore sandbar migration beneath moderate and energetic waves. The comparison showed wave-undertow interaction playing a crucial role in cross-shore sediment transport. Waves increased the undertow-induced suspended-load flux during offshore sandbar migration, and a weak undertow suppressed the wave-induced onshore bed-load transport during onshore sandbar migration. The proposed empirical time-dependent turbulent eddy viscosity significantly improved the prediction of onshore-directed bed-load transport during onshore sandbar migration. **DOI: 10.1061/(ASCE)WW.1943-5460.0000231.**

Author keywords: Sandbars; Waves; Undertow; Wave-current interaction; Sediment transport; Numerical models.

Introduction

Sandbars appear in many natural sandy coasts and inlets. Breaking-wave energy dissipation over the sandbars can serve as a natural mechanism for beach protection. Sandbars are highly dynamic with respect to their position and shape under varying hydrodynamic conditions at different spatial and temporal scales. However, behaviors of sandbars remain difficult to predict in practice because of an incomplete description of the underlying hydrodynamic mechanisms in numerical models. The objective of this study is to develop an improved process-based numerical model that can simulate sandbar migration for a better understanding of cross-shore profile evolution, which is extremely important in coastal engineering.

Literature Review

Numerical models for sandbar migration vary widely in their complexity. These range from behavior-oriented models (e.g., Plant et al. 1999) to process-based models (e.g., van Rijn et al. 2003). Behavior-oriented models use simple conceptual equations to predict sandbar position, and they are simple and useful but require site-specific data for model parameterization. Process-based models consider detailed underlying processes, but their predictability depends on the completeness of the physical mechanisms included. This study focuses on improvements of the process-based models.

The development of process-based models was prompted by recognition of the different roles of nonlinear waves and wave-induced undertow in sandbar migration. Gallagher et al. (1998) showed that undertow current moves sediments offshore, causing offshore sandbar migration under energetic wave conditions. Hoefel and Elgar (2003) suggested that stronger nonlinear waves drive onshore sediment transport and sandbar migration under moderate wave conditions. In the prototype environment, however, there is a complex interaction between high-frequency waves and low-frequency undertow such that sediment transport is controlled by the combined effects of both. Ruessink et al. (2011) showed in an analysis of laboratory measurements that an opposing current acting on an asymmetric wave could enhance sediment stirring during the negative-flow phase and resulted in a direction reversal of the wave-related sediment transport. The field measurements of Aagaard and Hughes (2010) showed that waves can enhance the bed shear stress and sediment suspension, thus affecting the magnitude of undertow-related transport. The preceding recent laboratory and field studies and reviewed literature suggested that wave-undertow interaction exhibits an obvious phase- and depth-dependent behavior and is an essential physical process that affects sediment transport and sandbar migration. The consequence of not properly considering wave-undertow interaction is thought be a primary reason that modelers do not reliably predict cross-shore profile behavior in prototype environments, which became the main motivation for this research.

On the other hand, a few process-based models for sandbar migration have considered nonlinear waves and undertow in different ways, but the mechanism of wave-undertow interaction has not been included. Hendersen et al. (2004) simulated the near-bed flow and sediment flux by solving the wave boundary-layer equation and sediment advection-diffusion equation with a two-equation turbulence

[1]Professor, State Key Laboratory of Hydrology–Water Resources and Hydraulic Engineering, Hohai Univ., Nanjing, 210098, China (corresponding author). E-mail: jhzheng@hhu.edu.cn

[2]Associate Professor, State Key Laboratory of Hydrology–Water Resources and Hydraulic Engineering, Hohai Univ., Nanjing, 210098, China.

[3]Research Hydraulic Engineer, U.S. Army Engineer Research and Development Center, Coastal and Hydraulics Laboratory, 3909 Halls Ferry Road, Vicksburg, MS 39180.

[4]Research Hydraulic Engineer, U.S. Army Engineer Research and Development Center, Coastal and Hydraulics Laboratory, 3909 Halls Ferry Road, Vicksburg, MS 39180.

Note. This manuscript was submitted on December 1, 2012; approved on July 31, 2013; published online on August 2, 2013. Discussion period open until August 1, 2014; separate discussions must be submitted for individual papers. This paper is part of the ***Journal of Waterway, Port, Coastal, and Ocean Engineering***, Vol. 140, No. 2, March 1, 2014. ©ASCE, ISSN 0733-950X/2014/2-146–159/$25.00.

J. Waterway, Port, Coastal, Ocean Eng. 2014.140:146-159.

closure model. The nonlinear wave effects were included by using the measured time series of near-bed velocity. A similar approach was reported by Hsu et al. (2006). These phase-resolving models represented a few wave-related transport mechanisms (e.g., phase lag between velocity and concentration), but the undertow effects were not properly represented because the mean-pressure-gradient term was neglected in the governing equation (Zhang et al. 2011). Consequently, this led to inaccurate net suspended-load estimation. In addition, neither the processes above the boundary layer nor the wave-breaking effects were considered in these types of models.

Other models (e.g., van Rijn et al. 2003; Spielmann et al. 2004; Ruessink et al. 2007) predicted the period-averaged undertow velocity and sediment concentration across the water depth using the period-averaged flow and sediment equations with a time-independent turbulent eddy viscosity formulation. The nonlinear wave effects were considered for the bed load, the suspended load was assumed to be purely related to undertow, but the wave-related contribution was not considered, which may result in considerable errors when the phase lag effects are significant. Consequently, wave-undertow interaction was not fully represented as a result of the period-averaged features of these models.

In summary, the reviewed literature indicated that previous sandbar migration models have commonly neglected the important process of wave-undertow interaction. This can be one of the main reasons why a reliable simulation of seasonal onshore-offshore sandbar migration under various wave and current conditions still remains a challenging task for the existing models (van Rijn et al. 2003). The objective of this study is therefore to develop an improved process-based model by including wave-undertow interaction, which requires the use of a phase- and depth-resolving approach. The authors accomplish this goal by introducing two important changes to the modeling approach: (1) using the first-order wave-current momentum equation that includes the undertow-related mean-pressure-gradient term (Zhang et al. 2011) and (2) proposing a time-dependent turbulent eddy viscosity formulation that is considered to be more physically sound and suitable for describing the intrawave velocity variation (Trowbridge and Madsen 1984). The authors have used extensive data from a large-scale laboratory experiment to validate this new model, investigated the sensitivity of model predictions to parameters, and examined the effects of wave-undertow interaction on sandbar migration.

Numerical Model

The present numerical model consists of four modules: wave module, flow module, sediment-transport module, and bed-evolution module. The integrated model simulates the cross-shore distribution of the period-averaged wave characteristics, roller energy, and wave setup, as well as the phase-resolving flow velocity, sediment concentration, bed load, and suspended load. Two new features included in the present model are the wave-undertow interaction and an empirical time-dependent turbulent eddy viscosity formulation. A brief description of the modules follows.

Wave Module

The random wave field is assumed to be narrow banded in frequency and unidirectional, which is a common approach for surf-zone wave modeling (Ruessink et al. 2007). The RMS wave height H_{rms} at each cross-shore location is calculated using the one-dimensional wave energy-balance equation

$$\frac{\partial(E_w c_g)}{\partial x} = -D_w \tag{1}$$

where E_w = wave energy; c_g = group velocity; x = horizontal coordinate (positive shoreward); and D_w = energy dissipation due to wave breaking. Dissipation is estimated based on Janssen and Battjes (2007). Linear wave theory is used to solve Eq. (1).

The breaking-induced surface roller is represented by the roller energy-balance equation (Stive and De Vriend 1994)

$$\frac{\partial(2E_r c)}{\partial x} = D_w - D_r \tag{2}$$

$$D_r = \frac{2gE_r \sin\beta}{c} \tag{3}$$

where E_r = roller energy; c = phase velocity; D_r = roller dissipation; g = gravitational acceleration; and β = roller slope.

The wave setup $\overline{\eta}$ is estimated using the depth-integrated and period-averaged momentum equation that includes the excess wave roller contribution

$$\frac{\partial S_{xx}}{\partial x} + \frac{\partial 2E_r}{\partial x} + \rho g(h+\overline{\eta})\frac{\partial \overline{\eta}}{\partial x} = 0 \tag{4}$$

where S_{xx} = wave radiation stress; ρ = water density; and h = still-water depth.

Flow Module

The intrawave flow velocity is modeled based on the following first-order wave-current momentum equation (Zhang et al. 2011):

$$\frac{\partial u}{\partial t} = \frac{\partial u_\infty}{\partial t} + \frac{\partial}{\partial z}\left[(v_t + v)\frac{\partial u}{\partial z}\right] - \frac{1}{\rho}\frac{\partial \overline{p}}{\partial x} - \frac{1}{\rho}\frac{\partial \overline{\tau}_{\text{bls}}}{\partial z} \tag{5}$$

where u = flow velocity; u_∞ = wave-induced free-stream velocity; v_t and v = turbulent and kinematic eddy viscosities, respectively; $\overline{p}$ = mean pressure; $\overline{\tau}_{\text{bls}}$ = additional mean shear stress induced by the bottom boundary-layer streaming; t = time; and z = vertical coordinate (positive upward with $z = 0$ at the bed).

On the right side of Eq. (5), the first and third terms represent the wave-induced oscillatory and undertow-induced mean horizontal pressure gradients, respectively. In the wave-induced pressure-gradient term, the authors used the representative free-stream velocity signal with the method of Elfrink et al. (2006) to describe the random wave-induced oscillatory motion. Absent any reliable theory for the random velocity signal, this approach is practically useful because it provides an equivalent wave force for nonlinear wave shape effects using wave parameters from the phase-averaged wave models. However, wave randomness effects are not represented, which requires use of more complex phase-resolving Boussinesq models or the measured near-bed velocity input. For the undertow-induced mean pressure gradient, Zhang et al. (2011) showed that this term is important for predicting the mean velocity and shear stress developed under breaking waves and currents. Using such formulation, wave and undertow are coupled, and the wave-undertow interaction is considered in a phase- and depth-resolving manner.

Eq. (5) is based on the first-order wave boundary-layer concept, and it is in principle only applicable inside the boundary layer. In this study, flow information in the upper water column is also required for predicting sandbar migration. The authors have used this equation across the water depth to obtain a solution of velocity both inside and outside the boundary layer. In doing so, the authors have assumed that the horizontal pressure gradient is constant over the depth. This assumption was necessary to develop a model for practical application at regional scale (e.g., large spatial domains and long-term

J. Waterway, Port, Coastal, Ocean Eng. 2014.140:146-159.

simulations). The flow equation used in this study is appropriate for shallow water depths, in which the surface variation–induced vertical velocity is small compared with the horizontal velocity. Because Eq. (5) is first order, the second-order effects (e.g., vertical velocity and the advection terms) are neglected, which may influence the morphodynamics by means of boundary-layer streaming, horizontal and vertical advection of fluid and sediment, and so on. A universal understanding of the relative importance of these mechanisms under different wave and seabed conditions is lacking. More comprehensive studies will be needed with a second-order model to fully address these issues. Consequently, the present model is suitable for local equilibrium conditions where advection is not the dominant process.

The streaming-induced mean-shear-stress gradient is valid in the bottom boundary layer and is expressed as (Reniers et al. 2004)

$$-\frac{1}{\rho}\frac{\partial \overline{\tau}_{\text{bls}}}{\partial z} = \begin{cases} \dfrac{D_f}{\rho c \delta} & (z \le \delta) \\ 0 & (z > \delta) \end{cases} \tag{6}$$

where δ = boundary-layer thickness; and D_f = energy dissipation owing to bottom friction. Both δ and D_f are estimated following the approach of Reniers et al. (2004).

Both the magnitude and the vertical profile of turbulent eddy viscosity in surf zone are difficult to parameterize. Various formulations of v_t have been used in previous studies by assuming that they are depth uniform or vary over the water column based on different profiles or shapes (Spielmann et al. 2004), whereas most of them are assumed to be time-independent within one wave cycle. If the intrawave velocity variation is considered, a time-dependent turbulent eddy viscosity is necessary (Trowbridge and Madsen 1984). Motivated by the great need for a physics-based estimation of the eddy viscosity, the authors introduce as a preliminary attempt a new empirical time-dependent eddy viscosity formulation

$$v_t = f_v H_{\text{rms}} \left(\frac{D_r}{\rho}\right)^{1/3} \frac{z}{h_t} \frac{\overline{|u_*^3|} + |u_*^3|}{\overline{|u_*^3|}} \tag{7}$$

$$u_* = \cos\varphi\, u_\infty + \sin\varphi \frac{1}{\omega}\frac{du_\infty}{dt} \tag{8}$$

where f_v = a constant; h_t = water depth below the wave trough level; and u_* = effective velocity that controls intrawave variation of eddy viscosity. The overbar denotes period averaging; φ is a phase-shift angle; and ω is the angle frequency. The present formulation [Eq. (7)] has the following features: (1) v_t is related to the roller energy dissipation (thus the breaking turbulence effects are considered), (2) v_t increases linearly from the bed to the wave trough level where the turbulence intensity is generally the highest, (3) the intrawave variation of v_t depends on both the wave-induced free-stream velocity and acceleration, whereas the relative importance of these is determined by φ, and (4) the period- and depth-averaged v_t is equivalent to the parameterization of Battjes (1975). The expression of u_* [Eq. (8)] is the same as the friction-velocity formulation of Nielsen and Callaghan (2003) used in the study of bed shear stress under skewed and asymmetric waves. This novel approach is used in this study to describe the phase dependency of turbulent eddy viscosity.

In principle, the near-bed wave-current boundary layer would be better solved with a detailed two-equation turbulence closure. This has been shown in the previous one-dimensional vertical (1DV) boundary-layer models of Hendersen et al. (2004), Hsu et al. (2006), and Zhang et al. (2011). However, in this approach it is difficult to consider the effects of external wave breaking–induced turbulence on the boundary layer because the flow structure outside the boundary layer is not included in these models. Although wave breaking takes place near the surface, under strongly breaking waves, the breaking turbulence can penetrate downward to affect the boundary layer (Scott et al. 2009; Aagaard and Hughes 2010). In this study, the authors solve for the flow velocity both inside and outside the boundary layer in the surf zone by using an empirical turbulent eddy viscosity formulation that includes breaking effects for the whole water depth. The authors do this by assuming that the eddy viscosity is linearly distributed in the vertical direction and that the breaking effects are present throughout the depth. These assumptions have been used in other practical beach profile models (e.g., Spielmann et al. 2004). This formulation strikes a balance between physical completeness of processes and practicality and engineering feasibility of the proposed eddy viscosity formulation.

At each cross-shore location, the mean-horizontal-pressure gradient ($-1/\rho \partial \overline{P}/\partial x$) in Eq. (5) is solved using an iterative algorithm requiring the mean flow flux to satisfy the period-averaged and depth-integrated mass-balance equation

$$\frac{1}{T}\int_0^T \int_0^{h_t} u\, dz dt + Q_w + Q_r = 0 \tag{9}$$

$$Q_w = \frac{1}{12}\frac{g}{c} H_{\text{rms}}^2 \tag{10}$$

$$Q_r = \frac{2E_r}{\rho c} \tag{11}$$

where T = wave period; and Q_w and Q_r = mass fluxes owing to wave and roller, respectively. In Eq. (10), the coefficient of $1/12$ is used to account for the effect of wave nonlinearity compared with $1/8$, which corresponds to linear waves.

To solve Eq. (5), the nonslip condition is applied at the bed, and the shear-stress condition is used at the wave trough level (Deigaard 1993)

$$u = 0 \quad (z = z_0 = k_s/30) \tag{12}$$

$$\tau = \frac{D_r}{c} \quad (z = h_t) \tag{13}$$

where k_s = bed roughness, taken as $2.5d_{50}$ in which d_{50} is the median grain size of sediment.

The present flow module describes the phase- and depth-resolving flow motion that takes into account the nonlinear waves, undertow, and bottom boundary-layer streaming, the three important processes essential for modeling cross-shore sediment transport and beach profile evolution (e.g., Gallagher et al. 1998; Hoefel and Elgar 2003; Hendersen et al. 2004; Kuriyama 2010). The simulated intrawave bed shear stress and flow velocity are used to drive the sediment-transport module.

Sediment-Transport Module

The period-averaged total sediment-transport rate is expressed as

$$\overline{q}_t = \overline{q}_b + \overline{q}_s \tag{14}$$

where q_t, q_b, and q_s = instantaneous total, bedload, and suspended load-transport rates, respectively.

J. Waterway, Port, Coastal, Ocean Eng. 2014.140:146-159.

Following Hsu et al. (2006) and Ruessink et al. (2007), the Meyer-Peter-Mueller formula (Ribberink 1998) is used here for the instantaneous bed-load transport rate as a function of the Shields parameter (θ):

$$q_b = 11\beta_s \frac{\theta}{|\theta|}(|\theta| - \theta_{cr})^{1.65}\sqrt{(s-1)gd_{50}^3} \tag{15}$$

$$\theta = \frac{\tau_b}{\rho(s-1)gd_{50}} \tag{16}$$

where τ_b = instantaneous bed shear stress; s = density ratio between sediment and water ($s = 2.65$); β_s = bed-slope correction factor that hinders upslope transport and favors downslope transport, representing the gravity effects of sediment particles over a sloping bed; and θ_{cr} = slope-corrected critical Shields parameter, below which no sediment movement is considered to take place. The expressions of β_s and θ_{cr} are, respectively, written as (van Rijn 1993; Ruessink et al. 2007)

$$\beta_s = \frac{\tan\phi}{\tan\phi + \dfrac{\tau_b}{|\tau_b|}\dfrac{\partial z}{\partial x}} \tag{17}$$

$$\theta_{cr} = \left\{\frac{\sin\left[\phi + \arctan\left(\dfrac{\tau_b}{|\tau_b|}\dfrac{\partial z}{\partial x}\right)\right]}{\sin\phi}\right\} \times \begin{cases} 0.24D_*^{-1} & 1 < D_* \le 4 \\ 0.14D_*^{-0.64} & 4 < D_* \le 10 \\ 0.04D_*^{-0.1} & 10 < D_* \le 20 \\ 0.013D_*^{0.29} & 20 < D_* \le 150 \\ 0.055D_* & D_* > 150 \end{cases} \tag{18}$$

where ϕ = bed repose angle ($\phi = 30°$); and D_* = nondimensional grain size $\{D_* = d_{50}[g(s-1)/\nu^2]^{1/3}\}$.

The instantaneous suspended-load transport rate is expressed by integrating the product of sediment concentration and flow velocity over the depth

$$q_s = \int_{z_a}^{h_t} uc\, dz \tag{19}$$

where c = sediment concentration; and z_a = near-bed reference height defined as $2d_{50}$. The temporal and spatial variations in suspended sediment concentration are solved with the vertical advection-diffusion equation

$$\frac{\partial c}{\partial t} = w_s\frac{\partial c}{\partial z} + \frac{\partial}{\partial z}\left(\varepsilon_s\frac{\partial c}{\partial z}\right) \tag{20}$$

where w_s = settling velocity of suspended sediment; and ε_s = sediment diffusivity. Similar to Eq. (5), the second-order advection effects are ignored in Eq. (20), and this sediment equation is in principle suitable for local equilibrium conditions.

The settling velocity is computed according to van Rijn (1993) and reduced by hindered settling in an empirical way (Richardson and Zaki 1954):

$$w_s = w_{s0}\left(1 - \frac{c}{0.6}\right)^5 \tag{21}$$

where w_{s0} = settling velocity in clear water. van Rijn (2007) suggested that the suspended sediments are generally finer than the original bed by a rough relationship of $d_s/d_{50} = 0.5-1$ (d_s is the mean grain size of suspended sediment) even for a relatively uniform bed. The authors note that the suspended sediment size also depends on the local hydrodynamic condition. In this study, d_s is calculated with the formula of van Rijn (2007) and is used in the estimation of w_{s0}.

The sediment diffusivity is related to the turbulent eddy viscosity through the Prandtl/Schmidt number σ_p and the turbulence-damping effects (van Rijn 1993):

$$\varepsilon_s = \frac{\overline{\nu}_t}{\sigma_p}\left[1 + \left(\frac{c}{0.6}\right)^{0.8} - 2\left(\frac{c}{0.6}\right)^{0.4}\right] \tag{22}$$

It is noted that the wave period-averaged eddy viscosity $\overline{\nu}_t$ is used in Eq. (22). Based on numerical computations, the authors found that using the time-dependent eddy viscosity [ν_t; see Eq. (7)] in Eq. (22) would lead to unrealistically high sediment concentration and suspended load flux during onshore sandbar migration, which are inconsistent with the measured data. Using field data for nonbreaking-wave bottom boundary layer, Foster et al. (2006) found that sediment suspension had an intermittent structure and was biased toward the onshore decelerating phase of the flow, whereas the turbulent kinetic energy was decreasing during this phase. Scott et al. (2009) reported that under breaking waves, for the erosive (accretive) conditions, only 33% (15%) of the total number of high-concentration events were correlated with the steep-wave events and the locally generated breaking-wave turbulence events. They suggested that the nonlocal advection of turbulence and sediment concentration prevailed during accretive conditions. These studies indicated that the intrawave variation of ε_s and sediment suspension may not be simply proportional to that of ν_t. The predicted high concentration during onshore sandbar migration using the time-dependent eddy viscosity is considered largely related to the neglect of advection effects in the present model. Consequently, the authors have used the wave period-averaged eddy viscosity in Eq. (22), which significantly improved the accuracy of the predictions as compared with data.

Two boundary conditions were used for Eq. (20). At the top boundary, sediment concentration is zero. Near the bottom, a reference sediment concentration c_a is specified at $z = z_a$ according to Zyserman and Fredsøe (1994):

$$c_a = \frac{0.331(\theta - \theta_{cr})^{1.75}}{1 + 1.034(\theta - \theta_{cr})^{1.75}} \tag{23}$$

Bed-Evolution Module

The period-averaged total sediment transport rate is used to estimate the bed evolution

$$\frac{\partial z_b}{\partial t} = -\frac{1}{1-p}\frac{\partial \overline{q}_t}{\partial x} \tag{24}$$

where z_b = bed elevation; and $p = 0.3$ = bed porosity.

Experimental Model

The cross-shore sediment transport experiment (CROSSTEX) experimental data of sandbar migration (Guannel 2009) are used in this study to validate the numerical model. The CROSSTEX experiment was conducted in a large-wave flume at the O. H. Hinsdale Wave Research Laboratory of Oregon State University in 2005. The experiment

J. Waterway, Port, Coastal, Ocean Eng. 2014.140:146-159.

consisted of four phases focusing on different processes involved in cross-shore sediment transport, including wave boundary layer and bed form, breaking turbulence and sediment suspension, sandbar migration, and swash-zone processes. The interest of the authors is limited to sandbar migration.

This laboratory flume was 104 m long, 3.7 m wide, and 4.6 m deep. Irregular waves of the Texel Marsen Arsloe (TMA) spectrum were generated by a flap-type wave maker and normally incident on a mobile barred beach with an initial average slope of 1/20. The beach was filled with well-sorted natural sands with a median grain size of $d_{50} = 0.22$ mm. Water surface elevation, flow velocity, and sediment concentration at fixed locations from the proximity of wave maker up to the inner surf zone were measured using 12 resistance-type wave gauges, 8 near-bottom wall-mounted acoustic Doppler velocimeters (ADVs), and colocated optical backscatter sensors (OBSs). A mobile cart that mounted 1 wave gauge, 8 ADVs, 7 OBSs, and 19 fiber-optic backscatter sensors (FOBSs) with a vertically moving frame also was employed at a specified location of interest for different runs. A typical experimental run lasted 15 min. The bathymetry was measured with a multiple transducer array (MTA) after each run. The total and suspended-sediment transport rates were obtained from the measured bed-elevation change and the measured velocity and concentration, respectively. The bed-load transport rate was assumed to be the difference between the two. Fig. 1 shows the experimental setup with the positions of wall-mounted instruments, in which the cross-shore coordinate x is defined as positive in the shoreward direction with its origin set at the wave maker. See Guannel (2009) for detailed information about this experiment and the data obtained.

Two major sandbar-migration events were investigated during the experiment (Fig. 2). The sandbar was first moved offshore from $x \approx 64$ m to $x \approx 61$ m under 3.5-h action of relatively energetic waves with a larger incident RMS height (0.42 m) and a shorter peak period (4 s). During the following 11.25 h, weak waves with a smaller height (0.21 m) and a longer peak period (8 s) resulted in an onshore movement of sandbar position from $x \approx 61$ m to $x \approx 68$ m. The data collected during these events were used to compare with the numerical model in the next section.

Comparison of Numerical Model and Experimental Measurements

Numerical Model Setup

A Crank-Nicholson type of implicit finite-difference scheme is employed to discretize the governing equations. The tridiagonal matrix algorithm (TDMA) method (Thomas 1949) combined with the Newton-Raphson iterative algorithm is applied to solve the nonlinear system of differential equations. A uniform mesh in the cross-shore direction was used with a grid spacing of 0.5 m. In the vertical direction, 100 stretched grids were distributed by allowing grid spacing to increase logarithmically from the bed to the wave trough level. In this way, a finer spatial resolution was obtained near the bed, where the vertical gradients are particularly high. These numerical schemes have been used successfully in previous studies of near-shore hydrodynamics and sediment transport (Zhang et al. 2011). The time steps for intrawave flow and sediment computation were 0.04 and 0.08 s for offshore and onshore migration, respectively. The time steps for morphologic update were 4 and 8 s for offshore and onshore migration, respectively. The measured wave height and mean water level at $x = 49$ m were used to drive the model given that sediment transport and bathymetric change were active only shoreward of this location. Using the inputs of incident wave parameters and the beach profile, wave propagation and roller evolution are simulated at each time step. The flow and sediment-transport models are then solved to obtain the bed-elevation change in each time step. The updated beach profile is fed back to the wave and roller models for calculations to be performed in the next time step.

The model calibration parameters include the roller slope β, the scaling constant f_v, and the phase-shift angle φ for turbulent eddy viscosity and the Prandtl/Schmidt number σ_p. The values of calibrated parameters are listed in Table 1. It is noted that the authors did not intend to seek the same parameter set for both cases. These two tests cannot demonstrate the general model predictability. In addition, the authors did not use a parameter-optimization algorithm, as in the studies of Ruessink et al. (2007), which was not considered because in this study the authors deal with multiple issues, including the prediction of bed evolution, wave height, flow velocity, sediment concentration and transport rates, and so on. The parameters values in Table 1 provided good predictions of hydrodynamics and morphodynamics for both cases. Further parameter tuning will not affect the main findings of this study.

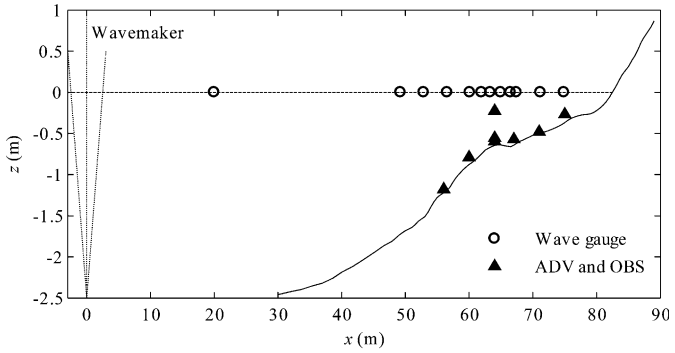

Fig. 1. Experimental setup with positions of wall-mounted instruments

Offshore Sandbar Migration Results

Fig. 3 shows model-predicted wave height, wave setup, undertow velocity, wave-velocity skewness, wave-velocity asymmetry, sediment concentration, suspended-load transport rate, bed-load transport rate, total transport rate, and beach profile evolution. Measured (circles and dotted lines) and modeled (solid lines) results are presented in Figs. 3(a–j) for the offshore sandbar migration and in Figs. 3(k–t) for the onshore sandbar migration. The RMS wave height is shown in Figs. 3(a and k) and wave setup in Figs. 3(b and l). The depth-averaged undertow velocity is shown in Figs. 3(c and m), wave-velocity skewness in Figs. 3(d and n) [estimated according to Hendersen et al. (2004)], and wave-velocity asymmetry in Figs. 3(e and o) [estimated according to Hendersen et al. (2004)]. The depth-integrated sediment concentration is shown in Figs. 3(f and p), suspended-load transport rate in Figs. 3(g and q), bed-load transport rate in Figs. 3(h and r), and total transport rate in Figs. 3(i and s). The initial (dash-dotted lines), measured final (dotted lines), and modeled final (solid lines) beach profiles are shown in Figs. 3(j and t). Because velocity and concentration profiles data were not available from Guannel (2009), profile validation will be addressed in the next phase of this research, which is necessary to determine the model's ability to predict the vertical variation of velocity and sediment concentration. In this first phase of this research, the authors' focus was on the model's ability to predict the cross-shore distribution of waves, undertow, asymmetry, and skewness of velocity and

J. Waterway, Port, Coastal, Ocean Eng. 2014.140:146-159.

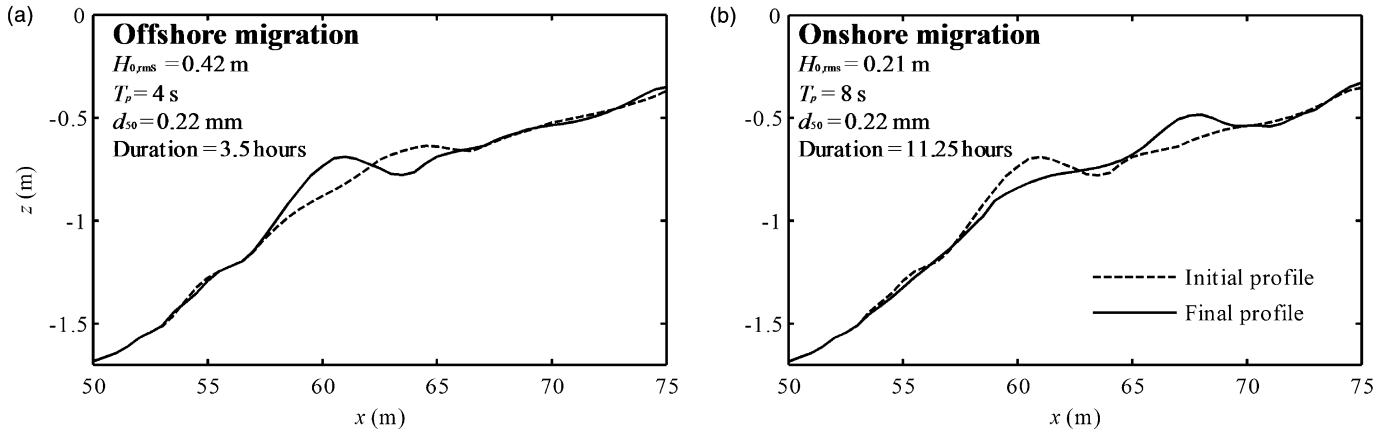

Fig. 2. Initial and final beach profiles and corresponding experimental conditions for (a) offshore and (b) onshore sandbar migration

Table 1. Model Parameters

Case	β	f_v	φ	σ_p
Offshore migration	0.15	0.030	30°	0.7
Onshore migration	0.10	0.055	30°	0.7

bed-load and suspended-sediment transport. Good model-data agreement was obtained and suggests that this model is capable of representing important physical mechanisms that drive onshore-offshore sandbar migration.

For the case of offshore sandbar migration, the breaking point appears in Fig. 3(a) at the seaward bar flank ($x \approx 60$ m). The predictions of wave height and setup agree well with the measurements [Figs. 3(a and b)]. The predicted undertow velocity is closely related to breaking-wave dissipation and has a peak slightly shoreward of the breaking point [Fig. 3(c)], which is the result of the spatial lag effect of breaking roller evolution. Figs. 3(d and e) show comparisons between modeled and measured wave-velocity skewness and asymmetry. It is noted that the wave seiching effects, which may affect wave skewness (Scott et al. 2009), are not considered in this model and also have been removed from the measured data presented here (Guannel 2009).The measured velocity skewness increases from offshore to the breaking point as a result of shoaling and remains rather uniform across the surf zone [Fig. 3(d)]. The model produces a reverse trend of this in the shoaling zone but gives accurate estimates in the surf zone. On the other hand, there is a modest increase in the velocity asymmetry over the entire profile that is captured correctly by the model [Fig. 3(e)]. This phenomenon suggests that wave shoaling leads to an increase in both velocity skewness and asymmetry, whereas the broken waves maintain a fairly constant shape. Intensive sediment suspension induced by wave breaking ($x \approx 60-65$ m) in the experiments was modeled accurately [Fig. 3(f)]. Predictions and data agree, showing that the maximum sediment suspension occurs at the same location as the maximum undertow and resulting in a large offshore-directed suspended-load flux [Fig. 3(g)]. Because of the saturation of broken waves, the sediment concentration and suspended-load transport rate gradually decrease toward the shoreline. The model accurately reproduces the slight onshore bed-load transport on the seaward side of the bar ($x \approx 50-58$ m) as a result of wave nonlinearities, as well as the offshore bed-load transport in the surf zone from undertow [Fig. 3(h)]. The simulated total-sediment transport rate has a consistent cross-shore distribution with the measurement [Fig. 3(i)]. It is shown that offshore sandbar migration [Fig. 3(j)] essentially resulted from the local gradient of offshore-directed sediment transport rate over the bar. The similar profiles obtained for the total transport rate and the undertow suggest that undertow is the dominant force responsible for this event. Numerical model results show that suspended load plays a major role in transport processes near the breaking point. In the inner surf zone, both bed and suspended loads are equally important.

Onshore Sandbar Migration Results

Less wave breaking occurred during onshore sandbar migration compared with the former case, resulting in smaller wave setup and a weaker undertow [Figs. 3(k–m)]. Unlike the former case, the undertow velocity gradually increases in the shoreward direction, reaches a peak located at the upper beach profile, and is without a local increase over the bar [Fig. 3(m)]. This indicates that fewer waves are breaking when they propagate through the bar. The calculated wave height, setup, and undertow are in agreements with the data. Figs. 3(n and o) show that the measured velocity asymmetry is approximately two times higher than its value during offshore migration, whereas the velocity skewness for both cases is comparable. This implies that wave asymmetry may be more important in driving onshore sandbar migration in this case. The cross-shore distributions of nonlinear velocity parameters in this case exhibit a close dependence on the bathymetry. As shown in Fig. 3(n), the velocity skewness decreases from the seaward boundary toward the seaward flank of the initial bar ($x \approx 50-60$ m), and then it increases over the initial bar and decreases over the area of final bar position ($x \approx 60-70$ m), which is the region of active sandbar migration. After the final bar, velocity skewness increases toward the shoreline. Although model-data discrepancy occurs in the shoaling region, the model correctly produces the overall variation in velocity skewness. The measured velocity asymmetry continuously increases from offshore and reaches its maximum shoreward of the final bar crest ($x \approx 67$ m) and then decreases toward the shoreline [Fig. 3(o)]. The model provides an accurate magnitude of velocity asymmetry over most of the profile.

Compared with the case of offshore migration, the sediment concentration and offshore-directed suspended-load transport rate (both measured and modeled) are less and concentrated at the region shoreward of the final bar ($x \approx 72$ m) [Figs. 3(p and q)], where breaking intensity and undertow velocity are relatively high. Over the active sandbar migration region ($x \approx 60-70$ m), little or no sediment is suspended and transported. Consequently, the total-sediment transport [Fig. 3(s)] is dominated by the onshore-directed

J. Waterway, Port, Coastal, Ocean Eng. 2014.140:146-159.

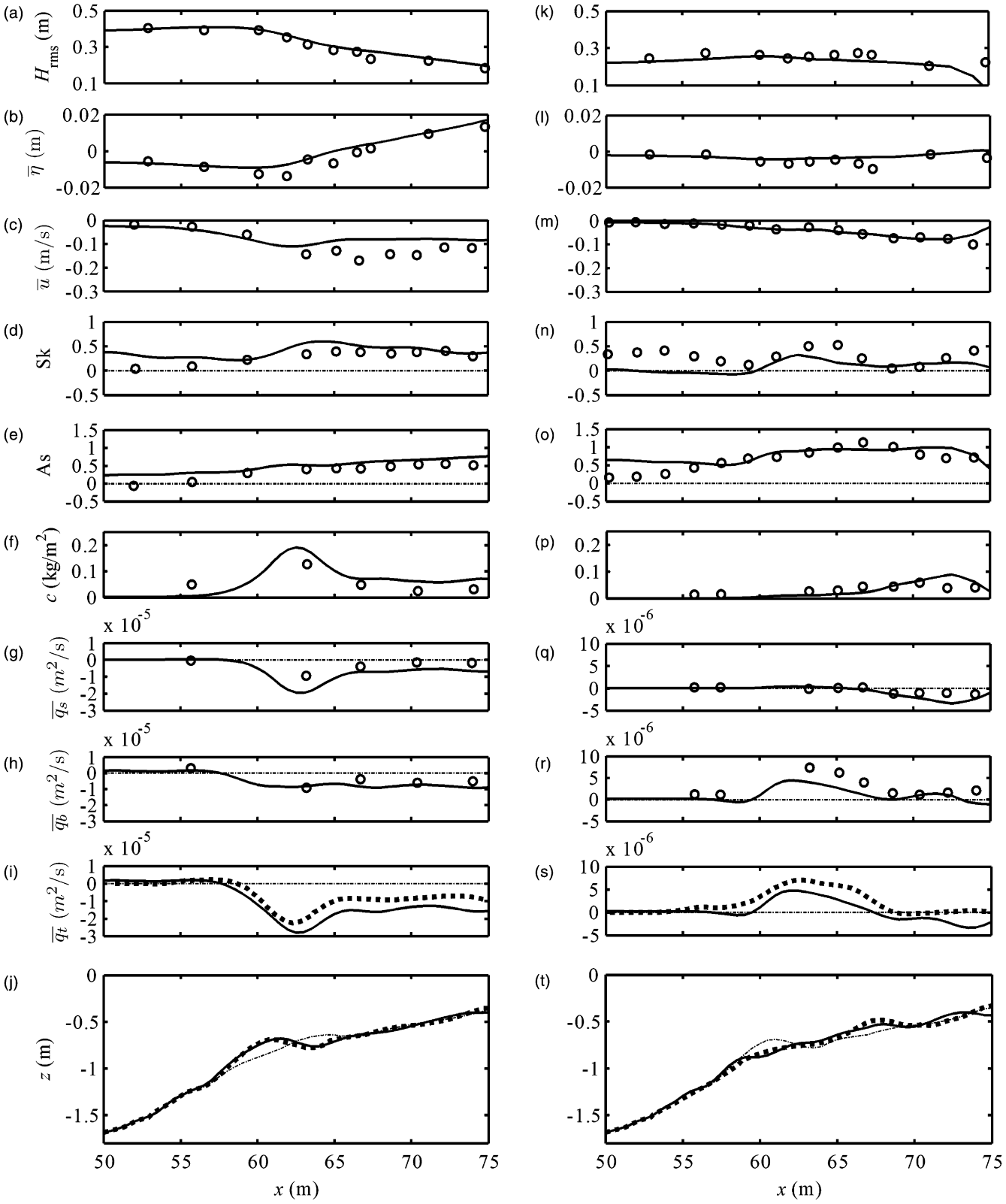

Fig. 3. Measured (circles and dotted lines) and modeled (solid lines) results: (a–j) offshore sandbar migration; (k–t) onshore sandbar migration

bed-load transport [Fig. 3(r)]. The onshore transport mainly appears at $x \approx 60-68$ m, where both velocity skewness and asymmetry are relatively high. It is noted that for this case, the bed load and suspended load are oppositely directed. In general, the model well reproduces the magnitude, direction, and cross-shore variation in sediment transport rates, leading to an accurate prediction of onshore bar migration [Fig. 3(t)]. It is found that the transport rate during onshore migration is much smaller than that during offshore migration. The model shows that onshore bed-load transport driven by wave nonlinearities is the dominant process.

J. Waterway, Port, Coastal, Ocean Eng. 2014.140:146-159.

Prediction of Wave- and Undertow-Related Transport

The authors investigated the individual effects of wave and undertow on suspended-load transport, as discussed in previous studies (e.g., Grasso et al. 2011). The total suspended-sediment transport rate is separated into the oscillatory wave-related and mean undertow-related transport rates with the following expression (van Rijn 1993):

$$\overline{q}_s = \int \overline{uc}\, dz = \underbrace{\int \overline{\tilde{u}\tilde{c}}\, dz}_{q_{s,w}} + \underbrace{\int \overline{u}\,\overline{c}\, dz}_{q_{s,c}} \tag{25}$$

where $q_{s,w}$ and $q_{s,c}$ = wave- and undertow-related transport rates, respectively. Fig. 4 shows for both cases that suspended-load flux is dominated by undertow-related transport and that wave-related transport is less important. For offshore sandbar migration [Fig. 4(a)], wave-related transport is onshore-directed at $x < 65$ m, and then it shifts to become offshore-directed at $x > 65$ m. This can be explained by the following mechanisms: for medium sands considered in this study, skewed and asymmetric waves tend to drive onshore-directed net suspended flux by stirring more sand during the positive flow phase than the negative flow phase. However, when an opposing undertow is present, it will decrease (increase) sand stirring during the positive (negative) flow phase, which tends to reduce wave-related onshore transport. If such an undertow is sufficiently strong, it even changes the wave-related transport direction from onshore to offshore, as observed by Ruessink et al. (2011). Therefore, in the region ($x < 65$ m) where waves are relatively strong, wave-related transport is onshore directed. Further into the surf zone, waves decay as a result of breaking, and undertow grows up, resulting in a direction reversal of the wave-related sediment transport at $x > 65$ m. For onshore sandbar migration [Fig. 4(b)], wave-related transport is always onshore directed and has a peak at $x \approx 72.5$ m. For this case, undertow is much weaker, and therefore, wave-related transport is dominated by wave nonlinearity and is onshore directed. In general, the magnitude of wave-related transport rate increases when both strength of flow and sediment concentration increase, as depicted at $x \approx 60-65$ m in Fig. 3(f) and $x \approx 70-75$ m in Fig. 3(p).

Discussion

Interaction of Nonlinear Waves and Undertow

This model considers wave-undertow interaction, which enables the authors to investigate the combined effects of wave and undertow on sediment transport. Whereas undertow (waves) has been identified as the dominant mechanism for offshore (onshore) sandbar migration, it is of particular interest to look at the role of waves (undertow) during offshore (onshore) sandbar migration. The authors do this by comparing the present numerical results, including wave-undertow interaction, with results that exclude wave (undertow) effects for investigating offshore (onshore) sandbar migration. The wave effects can be excluded by eliminating the wave pressure term and the boundary-layer streaming term in Eq. (5) and by using a time-invariant turbulent eddy viscosity. The undertow effects can be excluded by eliminating the mean-pressure-gradient term in Eq. (5). If undertow is neglected, Eq. (9) is not solved because the cross-shore mass balance is not required, and the zero-flux condition is applied at the top boundary to yield realistic results.

In Fig. 5, modeled results are presented for wave-undertow interaction (solid lines) and undertow only (dashed lines) in Figs. 5(a–f) for offshore sandbar migration and for wave only (dashed lines) in Figs. 5(g–l) for onshore sandbar migration. Figs. 5(a and g) show absolute values of the crest (bold lines) and trough (thin lines) Shields parameters θ_c and θ_t; Figs. 5(b and h) provide depth-integrated sediment concentration; Figs. 5(c and i) show suspended-load transport rate; Figs. 5(d and j) show the bed-load transport rate; Figs. 5(e and k) show the total transport rate; and Figs. 5(f and l) display beach profile evolution, in which the measured initial and final profiles are plotted with dash-dotted lines and dotted lines, respectively. Figs. 5(a–f) show the comparisons between modeled results with wave-undertow interaction and those with undertow only for offshore sandbar migration. Results indicate that the presence of waves increases remarkably both the crest and trough Shields parameters because of the increase of near-bed flow velocity. This leads to the enhanced sediment-suspension [Fig. 5(b)] and suspended-load transport [Fig. 5(c)], but as shown in Fig. 5(d), the offshore-directed bed-load transport rate is reduced considerably by waves over the bar ($x \approx 60-65$ m). This is caused by wave nonlinearities that

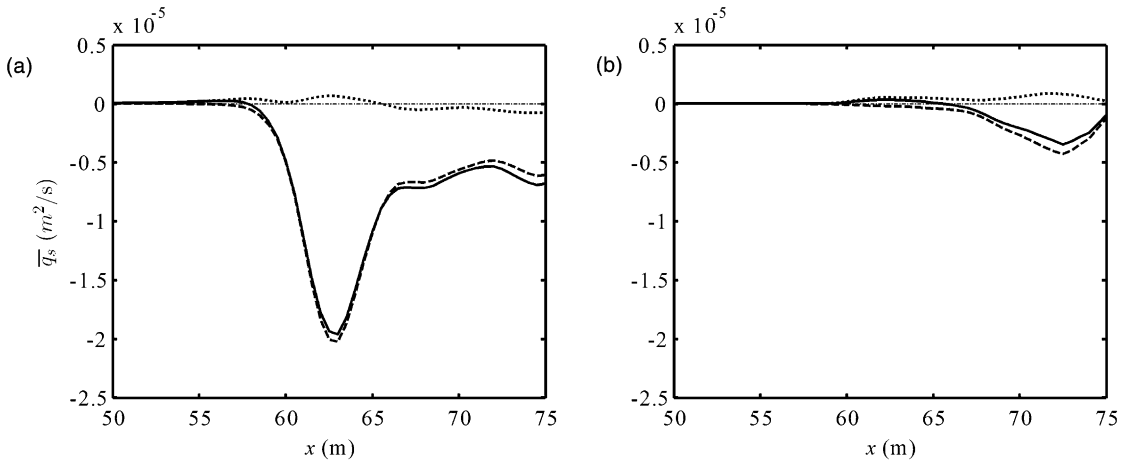

Fig. 4. Modeled results of wave-related (dotted lines), undertow-related (dashed lines), and total (solid lines) suspended-load transport rates: (a) offshore sandbar migration; (b) onshore sandbar migration

J. Waterway, Port, Coastal, Ocean Eng. 2014.140:146-159.

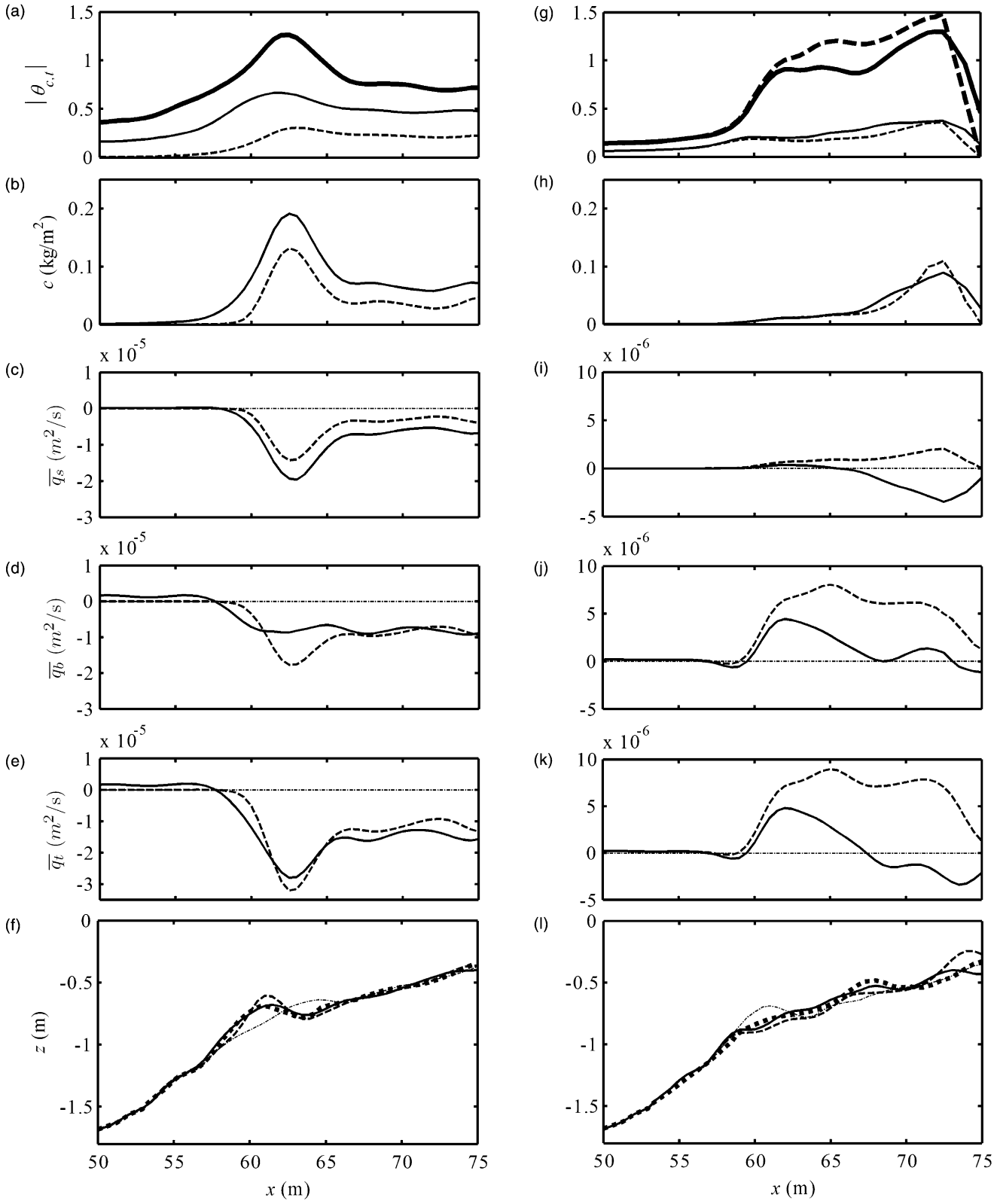

Fig. 5. (a–f) Modeled results for wave-undertow interaction (solid lines) and undertow only (dashed lines) for offshore sandbar migration and (g–l) for wave only (dashed lines) for onshore sandbar migration

tend to produce onshore-directed bed-load transport, given that θ_c is greater than θ_t in this region [Fig. 5(a)]. For the case of wave-undertow interaction, although θ_c is larger than θ_t over the entire profile, the bed-load transport is mostly offshore directed. Because both θ_c and θ_c are large enough to move sediment, the offshore-directed bed-load transport resulted from the longer duration of the negative-flow phase than the positive-flow phase under skewed waves and opposing undertow. Based on a laboratory observation,

J. Waterway, Port, Coastal, Ocean Eng. 2014.140:146-159.

Grasso et al. (2011) showed that under the conditions that $\theta_c/\theta_t > 1$ and the undertow is weak, strong phase-lag effects associated with velocity skewness can dominate net offshore sediment transport. The present numerical model results indicate that under a relatively strong undertow, the condition of $\theta_c/\theta_t > 1$ can occur, and in this case, phase-lag effects are less important (shown in Fig. 4), and the net offshore transport is dominated by undertow. Because of the increase in suspended-load transport and the decrease in bed-load transport, the total transport with wave-undertow interaction is similar to the undertow-only case [Fig. 5(e)], and the predictions of beach profile evolution are similar for both cases [Fig. 5(f)].

For the case of onshore sandbar migration, the presence of undertow indeed reduces the crest Shields parameter and increases the trough Shields parameter [Fig. 5(g)], leading to a slightly decreased concentration peak [Fig. 5(h)]. As shown in Fig. 5(i), when undertow is not considered, the suspended-load transport is driven purely by waves and is onshore directed. Comparing Fig. 4(b) with Fig. 5(i), the authors note that undertow not only results in an offshore-directed total suspended-load transport but also reduces the magnitude of onshore-directed wave-related suspended flux. This observation is qualitatively consistent with the suggestion of Ruessink et al. (2011). In Figs. 5(j and k), although undertow is relatively weak in this case, the undertow suppresses significantly the wave-induced onshore bed-load transport and total transport. Notice that if values of θ_c/θ_t are high and θ_t is small compared with their values during offshore sandbar migration, most sediment transport occurs during the positive-flow phase. Consequently, the undertow-induced decrease in the onshore-directed bed-load transport is the result of a decrease in bed shear stress during the positive-flow phase. The simulation for the wave-only case overpredicts the onshore movement of the sandbar [Fig. 5(l)]. Based on results discussed in this section, the authors conclude that the combined influence of wave and undertow on sediment transport shows the presence of a strong wave-undertow interaction that should be properly included in numerical models for realistic simulations of near-shore sediment transport and sandbar migration.

Numerical Model Parameters

The calibration and sensitivity of model parameters are discussed in this section. The roller slope β affects the dissipation rate of surface roller, undertow velocity, and the local turbulence. The scaling constant f_v and the phase-shift angle φ affect the magnitude and intrawave varying pattern of turbulent eddy viscosity, respectively. The Prandtl/Schmidt number σ_p controls the amount of suspended sediment. According to Table 1, the values of f_v are comparable with those of previous studies (e.g., Reniers et al. 2004; Spielmann et al. 2004; Ruessink et al. 2007). A Prandtl/Schmidt number of less than unity is standard (van Rijn 1993). In this study, the authors

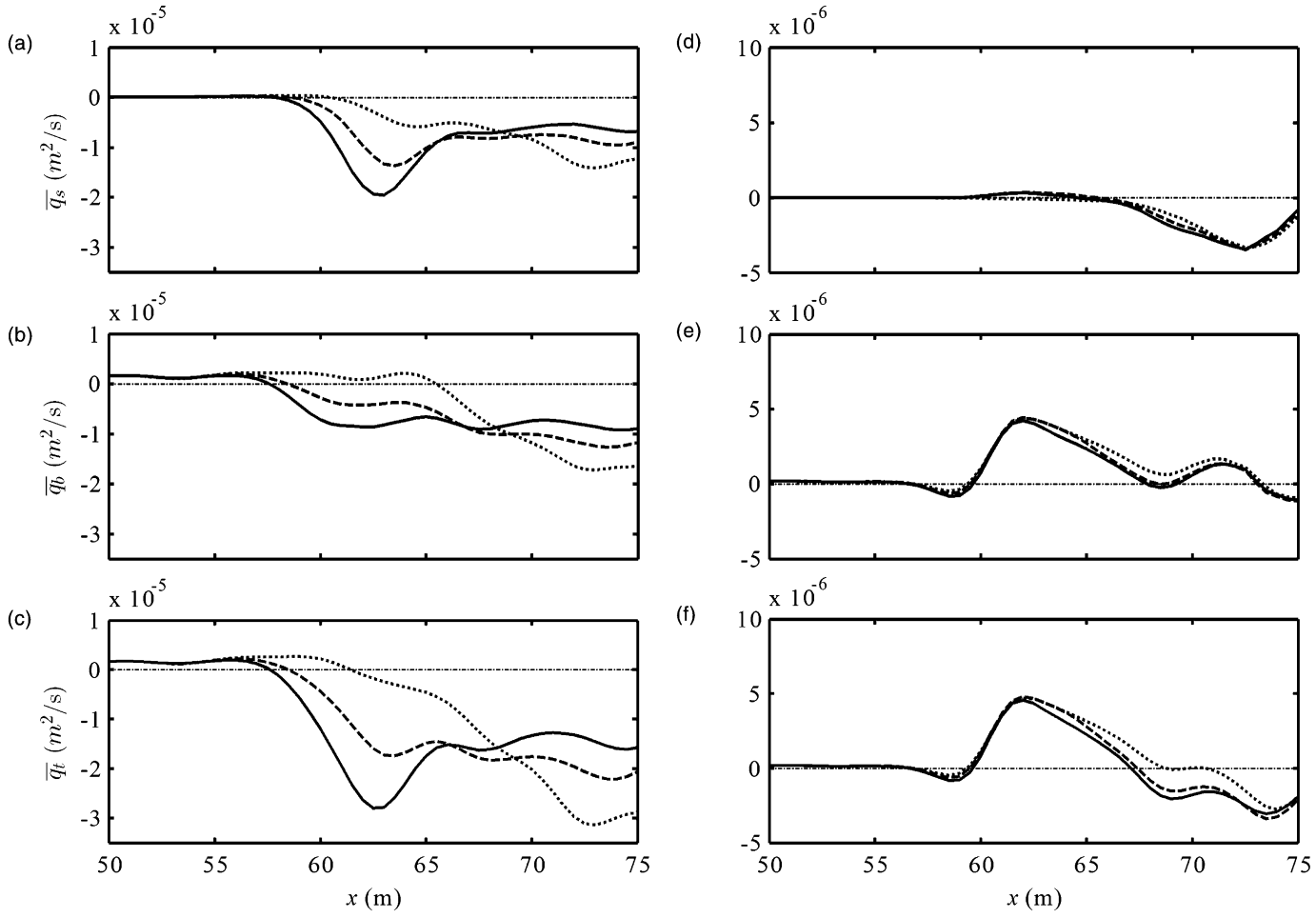

Fig. 6. Model results for offshore sandbar migration (a–c) and onshore sandbar migration (d–f) for suspended-load transport rate (a and d), bed-load transport rate (b and e), and total transport rate (c and f) for various values of roller slope

J. Waterway, Port, Coastal, Ocean Eng. 2014.140:146-159.

will focus on two remaining parameters that have not been investigated in detail previously.

The parameter $\beta = 0.1$ has been used in some studies (e.g., Reniers et al. 2004; Ruessink et al. 2007). Based on the remote sensing of roller dynamics in the laboratory, Haller and Catalán (2009) found that a remarkably greater $\beta\ (\approx 0.35)$ fitted best with measurements. The authors have investigated the effects of β in this study, and model results are provided in Fig. 6. Results for offshore sandbar migration are in Figs. 6(a–c), and onshore sandbar migration results are in Figs. 6(d–f). These include results for suspended-load transport rate [Figs. 6(a and d)], bed-load transport rate [Figs. 6(b and e)], and total transport rate [Figs. 6(c and f)] for $\beta = 0.05$ (dotted lines), $\beta = 0.1$ (dashed lines), and $\beta = 0.15$ (solid lines). The authors found that β has a weak influence on sediment transport during onshore sandbar migration and that larger β values are associated with increasing offshore-directed suspended-load transport rate and reduced bed-load transport rate [Figs. 6(d–f)]. Consequently, the total transport rate decreases with an increase in β. An important effect of β on sediment transport during offshore sandbar migration can be seen in Figs. 6(a–c). For large values of β, the suspended-load flux increases after the breaking point ($x \approx 60-65$ m) as a result of the locally enhanced roller dissipation, turbulence, and sediment suspension and decreases in the inner surf zone ($x > 70$ m) as a result of the more rapid decay of undertow current [Fig. 6(a)]. For the bed-load flux [Fig. 6(b)], high values of β tend to promote the offshore transport near the bar ($x \approx 57-68$ m) as a result of the increasing turbulence and bed shear stresses. At $x > 68$ m, the bed-load flux is stronger for small values of β because of strong undertow current in this region. For $\beta = 0.05$, the peak total transport rate occurs at the upper profile, and no appreciable sediment transport occurs over the bar. Based on these results, the authors conclude that the effects of roller slope in the present model depend on details of the local hydrodynamics and morphology. In general, too small values of β will fail to produce correct sediment-transport processes.

The phase-shift angle φ is a new parameter the authors have introduced in this morphodynamic model, but the authors have little guidance on how best to determine this parameter for practical applications. Indeed, the phase relationships between flow velocity and turbulence have been observed in field and laboratory (e.g., Foster et al. 2006; Scott et al. 2009; Aagaard and Hughes 2010). However, the data and knowledge are lacking, and different turbulence characteristics were reported with varying intermittency and negative and positive correlations for the fluid velocity. The variations depend on different breaking conditions and are associated with site-specific sediment transport mechanisms. The empirical time-dependent turbulent eddy viscosity formulation [Eq. (7)] introduced in this study describes the positive correlation between the velocity and turbulence intensity. This parameter promotes net onshore sediment transport. The intermittent features of turbulence, as well as the intrawave change in the eddy viscosity

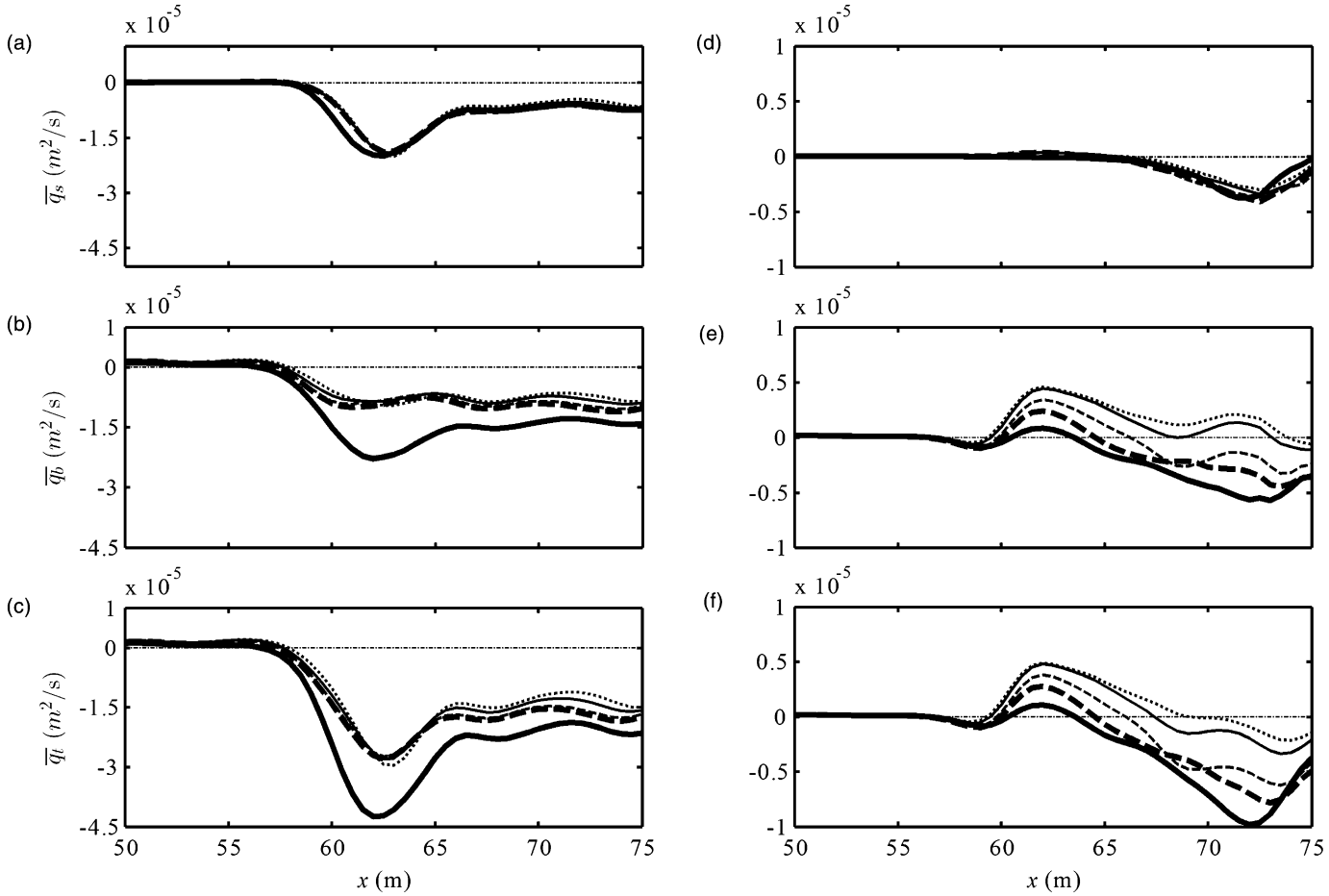

Fig. 7. Model results for offshore sandbar migration (a–c) and onshore sandbar migration (d–f) with conventional time-independent eddy viscosity formulation (bold solid lines) and new time-dependent eddy viscosity formulation for various values of phase-shift angle

J. Waterway, Port, Coastal, Ocean Eng. 2014.140:146-159.

profile owing to the vertical transport of both breaking- and bed-generated turbulence, were not considered in this research. The parameter φ may be interpreted as a calibration parameter that compensates partially the missing processes to yield improved modeling predictions. Nevertheless, the value of φ (30°) was adopted in this study, which is close to that (40°) used by Nielsen and Callaghan (2003), although this parameter is used to describe different mechanism here.

Fig. 7 provides model results for offshore sandbar migration [Figs. 7(a–c)] and onshore sandbar migration [Figs. 7(d–f)] using the conventional time-independent eddy viscosity formulation (bold solid lines) and the new time-dependent eddy viscosity formulation for $\varphi = 0°$ (bold dashed lines), $\varphi = 15°$ (thin dashed lines), $\varphi = 30°$ (thin solid lines), and $\varphi = 45°$ (dotted lines). Suspended-load transport rate results are in Figs. 7(a and d), bed-load transport rate in Figs. 7(b and e), and total transport rate in Figs. 7(c and f). For both onshore and offshore sandbars, the time-averaged suspended-load transport is not sensitive to the intrawave variation in eddy viscosity [Figs. 7(a and d)]. However, the time-dependent eddy viscosity description reduces the offshore-directed bed-load transport rate for offshore migration [Fig. 7(b)], similar to the results shown in Fig. 5(d). This indicates that the intrawave variation in eddy viscosity promotes onshore bed-load transport driven by wave nonlinearities. The value of φ has a negligible influence on sediment transport during offshore sandbar migration [Figs. 7(a–c)]. On the other hand, the onshore-directed bed-load transport rate during onshore sandbar migration increases when the time-dependent eddy viscosity formulation is used and also increases as φ increases [Figs. 7(e and f)]. The latter is so because the crest Shields parameter increases with increasing values of φ. In particular, it is found that using the conventional time-independent eddy viscosity formulation cannot satisfactorily reproduce the onshore-directed bed-load transport and fails to predict onshore sandbar migration. Although the present eddy viscosity formulation is empirical and contains parameters with uncertainties, as a preliminary attempt, it does show the significance of time-dependent eddy viscosity for an accurate modeling of wave-induced sediment transport and morphologic evolution.

A sensitivity test of the overall parameter set regarding the qualitative results was performed to obtain more insights into this model's behaviors. The calibrated parameters for the offshore- and onshore-directed cases are referred to as offshore parameters and onshore parameters, respectively. Figs. 8 and 9 present the results

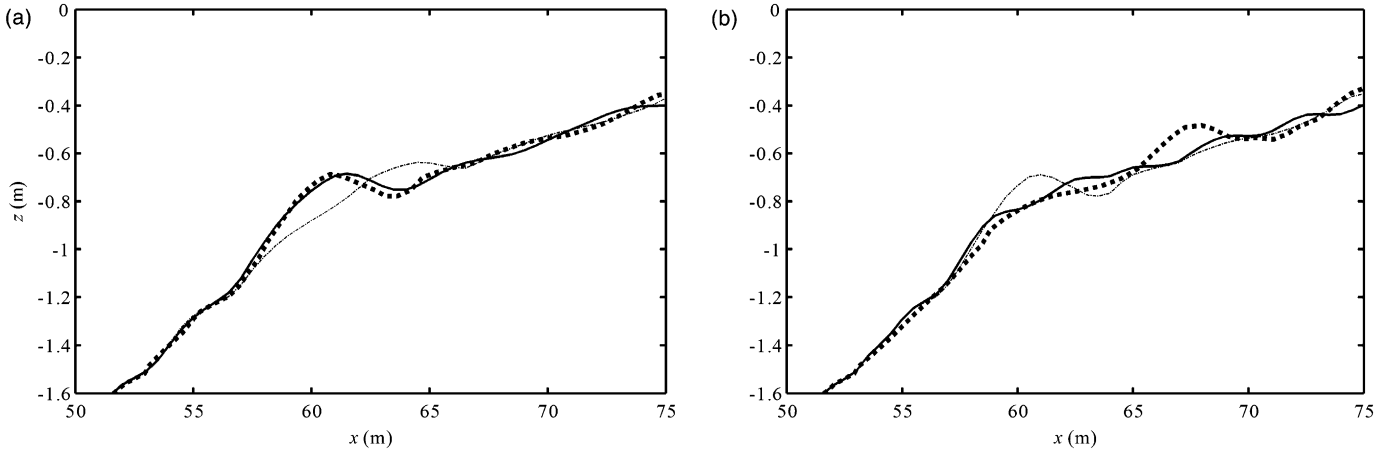

Fig. 8. Measured initial (dash-dotted lines), final (dotted lines), and modeled final (solid lines) beach profiles using offshore parameters: (a) offshore sandbar migration; (b) onshore sandbar migration

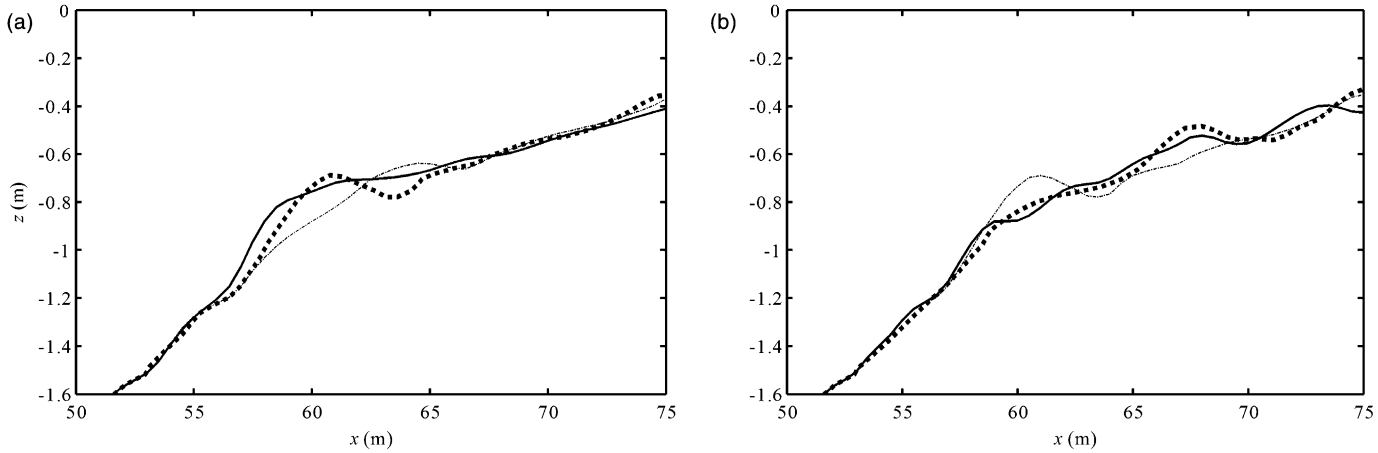

Fig. 9. Measured initial (dash-dotted lines), final (dotted lines), and modeled final (solid lines) beach profiles using onshore parameters: (a) offshore sandbar migration; (b) onshore sandbar migration

J. Waterway, Port, Coastal, Ocean Eng. 2014.140:146-159.

obtained using the same parameters for both sandbars. Although there are differences in the bar crest position and bar shape, the parameters initially calibrated for the offshore (onshore) sandbar also qualitatively reproduce the onshore (offshore) sandbar migration. This suggests the robustness and theoretical generalization of the proposed model.

Conclusions and Recommendations

The authors provide in this paper a new process-based sandbar migration model that includes wave-undertow interaction. Extensive model-data comparisons of wave height, setup, mean velocity, velocity skewness and asymmetry, sediment concentration, sediment transport rates, and bed-elevation change demonstrate the model's capability of predicting both onshore and offshore sandbar migration under moderate- and energetic-wave conditions. Results show that wave-undertow interaction significantly affects sediment transport and should be taken into account in sandbar migration modeling. Waves enhance the undertow-induced suspended-load flux by stirring more sediment into suspension during offshore sandbar migration. Even a weak undertow during onshore sandbar migration can significantly suppresses the wave-induced onshore bed-load transport by reducing the bed shear stress in the positive-flow phase. In addition, it is shown that the proposed empirical formulation of the time-dependent turbulent eddy viscosity greatly improves the prediction of onshore bed-load transport and sandbar migration compared with the conventional time-independent formulation.

The authors emphasize that the focus of this study was on development of a one-dimensional sandbar migration model in the cross-shore direction. Additional validation of this new model with field data from different sites is warranted to determine its suitability for a range of wave and current conditions. These tests should examine the sensitivity of cross-shore variation in the velocity and concentration profiles. Potential effects of spatial and temporal characteristics of site-specific undertow on the model's predictions ought to be investigated. The model should be expanded to two dimensions to account for the effects of wave-undertow interaction on sandbar evolution that occurs in real-world environment. Lastly, to extend the applicability of the model to advection-dominated processes, it will be necessary to include the advection effects in the model to accurately represent field conditions.

Acknowledgments

The authors gratefully acknowledge the O. H. Hinsdale Wave Research Laboratory at Oregon State University and Gregory Guannel for publishing the CROSSTEX experimental data, which were used for numerical model validation in this study. This work was supported by the National Natural Science Foundation of China (Grant No. 51209082, 51379071), the National Key Basic Research Development Program "973 Project" of China (Grant No. 2010CB429002), the National Key Technology Research and Development Program (Grant No. 2012BAB03B01), the 111 Project (Grant No. B12032), and the Qin Lan Project and 333 Project of Jiangsu Province (Grant No. BRA2012130). Zeki Demirbilek and Lihwa Lin are grateful for the technical support received in this activity from the U.S. Army Corps of Engineers Coastal Inlets Research Program (CIRP). The USACE Headquarters granted permission to publish this paper.

References

Aagaard, T., and Hughes, M. G. (2010). "Breaker turbulence and sediment suspension in the surf zone." *Marine Geol.*, 271(3–4), 250–259.

Battjes, J. A. (1975). "Modelling of turbulence in the surf zone." *Proc., Symp. on Modeling Techniques*, ASCE, Reston, VA, 1050–1061.

Deigaard, R. (1993). "A note on the three-dimensional shear stress distribution in a surf zone." *Coast. Eng.*, 20(1–2), 157–171.

Elfrink, B., Hanes, D. M., and Ruessink, B. G. (2006). "Parameterization and simulation of near bed orbital velocities under irregular waves in shallow water." *Coast. Eng.*, 53(11), 915–927.

Foster, D. L., Beach, R. A., and Holman, R. A. (2006). "Turbulence observations of the nearshore wave bottom boundary layer." *J. Geophys. Res.*, 111(C4).

Gallagher, E. L., Elgar, S., and Guza, R. T. (1998). "Observations of sandbar evolution on a natural beach." *J. Geophys. Res.*, 103(C2), 3203–3215.

Grasso, F., Michallet, H., and Barthélemy, E. (2011). "Sediment transport associated with morphological beach changes forced by irregular asymmetric, skewed waves." *J. Geophys. Res.*, 116(C3).

Guannel, G. (2009). "Observations of cross-shore sediment transport and formulation of the undertow." Ph.D. thesis, Oregon State Univ., Corvallis, OR.

Haller, M. C., and Catalán, P. A. (2009). "Remote sensing of wave roller lengths in the laboratory." *J. Geophys. Res.*, 114(C7).

Hendersen, S. M., Allen, J. S., and Newberger, P. A. (2004). "Nearshore sandbar migration predicted by an eddy-diffusive boundary layer model." *J. Geophys. Res.*, 109(C6).

Hoefel, F., and Elgar, S. (2003). "Wave-induced sediment transport and sandbar migration." *Science*, 299(5614), 1885–1887.

Hsu, T. J., Elgar, S., and Guza, R. T. (2006). "Wave-induced sediment transport and onshore sandbar migration." *Coast. Eng.*, 53(10), 817–824.

Janssen, T. T., and Battjes, J. A. (2007). "A note on wave energy dissipation over steep beaches." *Coast. Eng.*, 54(9), 711–716.

Kuriyama, Y. (2010). "A one-dimensional parametric model for undertow and longshore current velocities on barred beaches." *Coast. Eng. J.*, 52(02), 133–155.

Nielsen, P., and Callaghan, D. P. (2003). "Shear stress and sediment transport calculations for sheet flow under waves." *Coast. Eng.*, 47(3), 347–354.

Plant, N. G., Holman, R. A., Freilich, M. H., and Birkemeier, W. A. (1999). "A simple model for interannual sandbar behavior." *J. Geophys. Res.*, 104(C7), 15755–15776.

Reniers, A. J. H. M., Thornton, E. B., Stanton, T. P., and Roelvink, J. A. (2004). "Vertical flow structure during Sandy Duck: Observations and modeling." *Coast. Eng.*, 51(3), 237–260.

Ribberink, J. S. (1998). "Bed-load transport for steady flows and unsteady oscillatory flows." *Coast. Eng.*, 34(1–2), 59–82.

Richardson, J. F., and Zaki, W. N. (1954). "Sedimentation and fluidization. I." *Trans. of ICE*, 32, 35–53.

Ruessink, B. G., et al. (2011). "Observations of velocities, sand concentrations, and fluxes under velocity-asymmetric oscillatory flows." *J. Geophys. Res.*, 116(C3).

Ruessink, B. G., Kuriyama, Y., Reniers, A. J. H. M., Roelvink, J. A., and Walstra, D. J. R. (2007). "Modeling cross-shore sandbar behavior on the timescale of weeks." *J. Geophys. Res.*, 112(F3).

Scott, N. V., Hsu, T. J., and Cox, D. (2009). "Steep wave, turbulence, and sediment concentration statistics beneath a breaking wave field and their implications for sediment transport." *Cont. Shelf Res.*, 29(20), 2303–2317.

Spielmann, K., Astruc, D., and Thual, O. (2004). "Analysis of some key parametrizations in a beach profile morphodynamical model." *Coast. Eng.*, 51(10), 1021–1049.

Stive, M. J. F., and De Vriend, H. J. (1994). "Shear stresses and mean flow in shoaling and breaking waves." *Proc., 24th Int. Conf. on Coastal Engineering*, ASCE, Reston, VA, 594–608.

Thomas, L. H. (1949). "Elliptic problems in linear differential equations over a network." *Watson Scientific Computing Laboratory Rep.*, Columbia Univ., New York.

Trowbridge, J. H., and Madsen, O. S. (1984). "Turbulent wave boundary layers. 1: Model formulation and first-order solutions." *J. Geophys. Res.*, 89(C5), 7989–7997.

van Rijn, L. C. (1993). *Principles of sediment transport in rivers, estuaries, and coastal seas*, Aqua, Blokzijl, Netherlands.

van Rijn, L. C. (2007). "Unified view of sediment transport by currents and waves. II: Suspended transport." *J. Hydraul. Eng.*, 10.1061/(ASCE)0733-9429(2007)133:6(668), 668–689.

van Rijn, L. C., Walstra, D. J. R., Grasmeijer, B., Sutherland, J., Pan, S., and Sierra, J. P. (2003). "The predictability of cross-shore bed evolution of sandy beaches at the time scale of storms and seasons using process-based profile models." *Coast. Eng.*, 47(3), 295–327.

Zhang, C., Zheng, J. H., Wang, Y. G., and Demirbilek, Z. (2011). "Modeling wave-current bottom boundary layers beneath shoaling and breaking waves." *Geo-Mar. Lett.*, 31(3), 189–201.

Zyserman, J. A., and Fredsøe, J. (1994). "Data-analysis of bed concentration of suspended sediment." *J. Hydraul. Eng.*, 10.1061/(ASCE)0733-9429(1994)120:9(1021), 1021–1042.